UVicSPACE: Research & Learning Repository

University of Victoria

___

Faculty of Science

Faculty Publications

___

This is a post-print version of the following article:

Determining the Orientation of Chemical Functional Groups on Metal Surfaces by a Combination of Homodyne and Heterodyne Nonlinear Vibrational Spectroscopy

Wei-Chen Yang and Dennis K. Hore

November 2017

Determining the Orientation of Chemical Functional Groups on Metal Surfaces by a Combination of Homodyne and Heterodyne Nonlinear Vibrational Spectroscopy

Wei-Chen Yang and Dennis K. Hore*

Department of Chemistry, University of Victoria, Victoria, British Columbia, V8W 3V6, Canada

E-mail: dkhore@uvic.ca

1

Abstract

We illustrate how phase-sensitive sum-frequency generation spectroscopy may be used to determine the polar orientation of organic species on metals, where there is a significant electronic contribution to the second-order signal. It turns out that traditional direct heterodyne schemes—as would be applied to the same molecules on dielectric substrates—are challenging to use here as a result of the large resonant/non-resonant amplitude ratio that diminishes the phase contrast observed in tuning through the vibrational mode. This is demonstrated in a variety of experimental surfaces that illustrate all limiting cases. We propose a scheme that can overcome this challenge, and thereby determine the chemical functional group orientation through a combination of the homodyne spectrum, and some phase information from a heterodyne approach.

Introduction

Characterizing the structure of molecules attached to metal or semiconductor surfaces is a key step towards the understanding, optimization, and design of catalytic systems, solar cells, and corrosion inhibitors.[1–6] The manner in which molecules adsorb on the metal surface (the nature of their interaction to the surface, their orientation and polarity in the adsorbed state) determine the desired substrate functionality. In industrial applications such as corrosion inhibition, surfactant coatings are a critical frontline prevention for separating bare metal surfaces from oxygenated species. Such knowledge also provides mechanistic details to bottom-up manufacturing processes such as atomic layer deposition. Of all the techniques that are capable of characterizing molecules on surfaces, ones based on vibrational spectroscopy offer structural sensitivity and the ability to potentially recognize species based on the vibrational signature. However, conventional IR reflection absorption spectroscopy has limited, and often insufficient, sensitivity for low surface coverage. Nonlinear techniques such as visible-infrared sum-frequency generation (SFG) can offer the benefits of a vibrational optical probe, along with sensitivity to sub-monolayer concentrations.

As a direct consequence of the requirement of non-centrosymmetry to produce SFG signal, the phase of the emitted SFG field carries information on the polar orientation of surface chemical functional groups. By characterizing the phase in addition to the amplitude of the reflected SFG field, it is therefore possible to distinguish whether surface methyl groups, for example, are pointed towards the metal or towards the ambient air. Although several methods have been proposed for phase measurement in heterodyne SFG schemes,[7–23] such information does not strictly require explicit phase measurement. This is because metals often have large electronic (vibrationally non-resonant, NR) contributions to the SFG signal that constructively or destructively interfere with the SFG generated from the organic functional groups on IR resonance.[24,25] This interaction is much the same as achieved with an external phase reference (the local oscillator, LO) in a heterodyne experiment. Several studies have made use of this in the analysis of SFG data.[2,26–30] Explicit measurement of the phase has several advantages over reliance on implicit phase interpretation, primarily the result of being able to independently characterize, control, and modulate the LO

magnitude and phase. In this work we illustrate that, while heterodyne SFG measurements excel at measuring the phase of bare metals, and of organic layers adsorbed onto dielectric substrates with no appreciable NR response, there are challenges associated in phase characterization of organics on metals. We illustrate this with data from a bare aluminum surface, an organic alkyl surfactant on aluminum, alkyl functionalized glass, and an alkyl thiol on gold. After discussing the interplay between resonant and non-resonant responses for each surface, we present a straightforward method for determining the polarity of surface chemical functional groups using a combination of the heterodyne and homodyne SFG data.

Methods

Sample preparation. Aluminum coupons 1 mm thick were cut to 25 mm $\times$ 25 mm squares and both surfaces were rough finished using a milling machine. The samples were then polished by 320, 600, 1200 and 2000 grit papers in succession, each for 10 min. The polishing step was completed by using 3 μm diamond polishing suspension (Buehler MetaDi Supreme) for 15 min, followed by 0.05 μm alumina (Buehler Masterprep) for 15 min. Polished metal samples were washed with soap and rinsed in 18 MΩ·cm deionized water (Nanopure, Barnstead Thermo) for 10 min, and dried under nitrogen gas. The samples were then successively sonicated in acetone, ethanol, a second acetone step, and finally methanol, each for 30 min. The final treatment was exposure to oxygen plasma for 60 min. SFG spectra of these mirror finish Al pieces with strong specular reflection produced only non-vibrationally resonant signal. Sodium dodecyl sulfate 98% was purchased from Sigma-Aldrich and used without further purification. 0.014 M SDS solution was prepared in 18.2 MΩ·cm. The aluminum coupon was immersed into the solution for two hours then dried under nitrogen.

SFG data for tricholoro(octadecyl)silane monolayers on glass was obtained from a previous study;[19] those samples were prepared according to published methods.[31] The reagent (Aldrich, greater than 90% purity) was used without further treatment in a 4:1 solution of hexadecane and

CCl$_4$. Borosilicate glass microscope slides were cleaned in 110°C piranha for 1 h, rinsed with 18.2 MΩ·cm water, and dried under nitrogen. After immersing the clean substrates, unreacted OTS was removed by rinsing with chloroform, acetone, methanol, and water. The final step was drying at 80°C for 3 h. Similarly, SFG data for octadecane thiol (ODT) monolayers on gold was taken from Ref. 32. Those samples were prepared according to procedures described in an earlier report.[33] Substrates with 100 nm Au deposited on a 5 nm Cr adhesion layer (EMF, Ithaca, NY) were cleaned by sonication in acetone and ethanol, then immersed in 1×10^{-3} M solution of ODT in ethanol for 12 h. Any residual ODT was removed by soaking in fresh ethanol. Samples were subsequently dried under nitrogen.

Homodyne and heterodyne SFG spectroscopy. Our wavelength-scanning SFG system and its configuration for phase measurements has been described in Refs. 18 and 19. The essential details are that collinear 20 ps s-polarized visible (100 μJ/pulse) and p-polarized infrared (200 μJ/pulse) beams are incident at 70°. The local oscillator (LO) is generated in transmission before the sample in a 50 μm piece of y-cut quartz, oriented so that its optical axes are rotated only a few degrees from the plane of the incident beam polarizations. This simultaneously controls (reduces) the amount of LO generated to ensure sufficient contrast in the interference fringes,[18] and ensures that the polarization of the transmitted visible and infrared beams are not appreciably altered as a result of the quartz birefringence. Heterodyne data is collected by sequentially scanning the infrared frequency, and rotating a 1 mm fused silica plate that acts as a phase-shifting unit (PSU) between the sample and the y-cut quartz. These signals display temporal interference along the PSU rotation axis, and spectral interference along the IR frequency axis. After each experiment, the sample was replaced with a reference sample, a piece of z-cut quartz whose phase is known as a result of prior calibration.[19,34] In general, the bulk $\chi^{(2)}$ tensors of non-centrosymmetric crystals are real far from resonance, and have surface $\chi^{(2)}$ values that are shifted by 90° from the bulk. For our z-cut sample, we have marked the orientation of the crystal to produce $\phi_{\text{NR}} = -90°$. We have previously described the manner in which the sample and reference heterodyne data may be used together to arrive at the phase of the sample second-order susceptibility.[18,19]

Electronic structure calculations. We have considered a methyl group in three different chemical environments, next to an OH (methanol), in an ester group, and at the end of an alkyl chain (both ends of methyl hexanoate). Geometry optimization and subsequent Hessian calculation were performed in GAMESS using B3LYP/6-31G(d,p) and a PCM effective solvent model. Dipole moment and polarizability derivatives were then obtained using an explicit finite difference approach whereby the eigenvectors of the Hessian were used to construct seven input geometries that step along the methyl symmetric stretching normal mode. Full details of this procedure for estimating molecular hyperpolarizability tensor elements are given in Ref. 35.

Results & Discussion

Phase contrast in a heterodyne SFG experiment

We will show that the presence of a non-resonant contribution to $\chi^{(2)}$ that is significant compared to the resonant contribution effectively diminishes the phase contrast—the variation in phase upon passing through a vibrational resonance—as would be measured in a heterodyne SFG experiment. In the general case we have

$$\chi^{(2)} = \chi^{(2)}_{\mathrm{NR}} + \chi^{(2)}_{\mathrm{R}} = |\chi^{(2)}_{\mathrm{NR}} + \chi^{(2)}_{\mathrm{R}}|e^{i\phi}. \tag{1}$$

We illustrate the addition of $\chi^{(2)}_{\mathrm{NR}}$ and $\chi^{(2)}_{\mathrm{R}}$ in the complex plane in Fig. 1a. The graphic depicts the case where $|\chi^{(2)}_{\mathrm{NR}}| > |\chi^{(2)}_{\mathrm{R}}|$, and the dashed arrows indicate the phase trajectory of $\chi^{(2)}_{\mathrm{R}}$ as it passes from $0°$ to $180°$. At each value of ω_{IR}, the phase of the overall response in Eq. 1 is given by

$$
\begin{aligned}
\phi &= \arctan\left[\frac{|\chi^{(2)}_{\mathrm{NR}}|\sin\phi_{\mathrm{NR}} + |\chi^{(2)}_{\mathrm{R}}|\sin\phi_{\mathrm{R}}}{|\chi^{(2)}_{\mathrm{NR}}|\cos\phi_{\mathrm{NR}} + |\chi^{(2)}_{\mathrm{R}}|\cos\phi_{\mathrm{R}}}\right] \\
&= \arctan\left[\frac{R\sin\phi_{\mathrm{NR}} + \sin\phi_{\mathrm{R}}}{R\cos\phi_{\mathrm{NR}} + \cos\phi_{\mathrm{R}}}\right]
\end{aligned}
\tag{2}
$$

where $R \equiv |\chi_{NR}^{(2)}|/|\chi_R^{(2)}|$. The corresponding experimental observation is that there may be only a small change in ϕ upon passing through the vibrational resonance, compared to the 180° change when $\chi_{NR}^{(2)} = 0$. A graphical explanation for this may be seen in Fig. 1a. In order to observe the phase change in tuning ω_{IR} through this vibration, there must be a significant corresponding change in ϕ. We formally define the *phase contrast* as the largest difference in ϕ anywhere in the range $\phi_R = 0$–180° as the resonant mode undergoes a frequency-dependent phase change in the transition from $\omega_{IR} < \omega_0$ to $\omega_{IR} > \omega_0$.

$$\text{phase contrast} = \phi_{max}(\phi_{NR}, R; \phi_R) - \phi_{min}(\phi_{NR}, R; \phi_R) \tag{3}$$

Note that the best contrast is not necessarily measured pre- and post-resonance, nor does it occur pre- vs on-resonance. Rather, the phase contrast is a function of the ratio R and the value of the non-resonant phase ϕ_{NR}. This is shown in Fig. 1b, with some slices along R in Fig. 1c, and slices along ϕ_{NR} in Fig. 1d.

It is worthwhile to examine some limiting behaviors. When $|\chi_{NR}^{(2)}| \gg |\chi_R^{(2)}|$, that is when $R \to \infty$ the phase contrast approaches zero. This makes sense, as there is no variation in the phase in the absence of any molecular vibrations (or for modes that are not oriented in a polar manner at the surface), and $\phi \to \phi_{NR}$. In the other extreme, as the non-resonant amplitude becomes very small, $R \to 0$ and the phase contrast reaches its maximum value of 180°, irrespective of ϕ_R. The intermediate cases are of interest, as the contrast depends on both R and ϕ_{NR}. It is interesting to note that when $|\chi_{NR}^{(2)}| = |\chi_R^{(2)}|$ (when $R = 1$), the phase contrast is exactly 90°, irrespective of ϕ_{NR} (red curve in Fig. 1d). However, in the special case where $\phi_{NR} = 90°$, the phase contrast varies sharply for $R < 1$ and $R > 1$, as seen most clearly by the blue curve in Fig. 1c. In the case where $\phi_{NR} = 0°$ or 180°, the phase contrast always displays its maximum value of 180° if $R < 1$. We will now compare these predictions with some experimental observations.
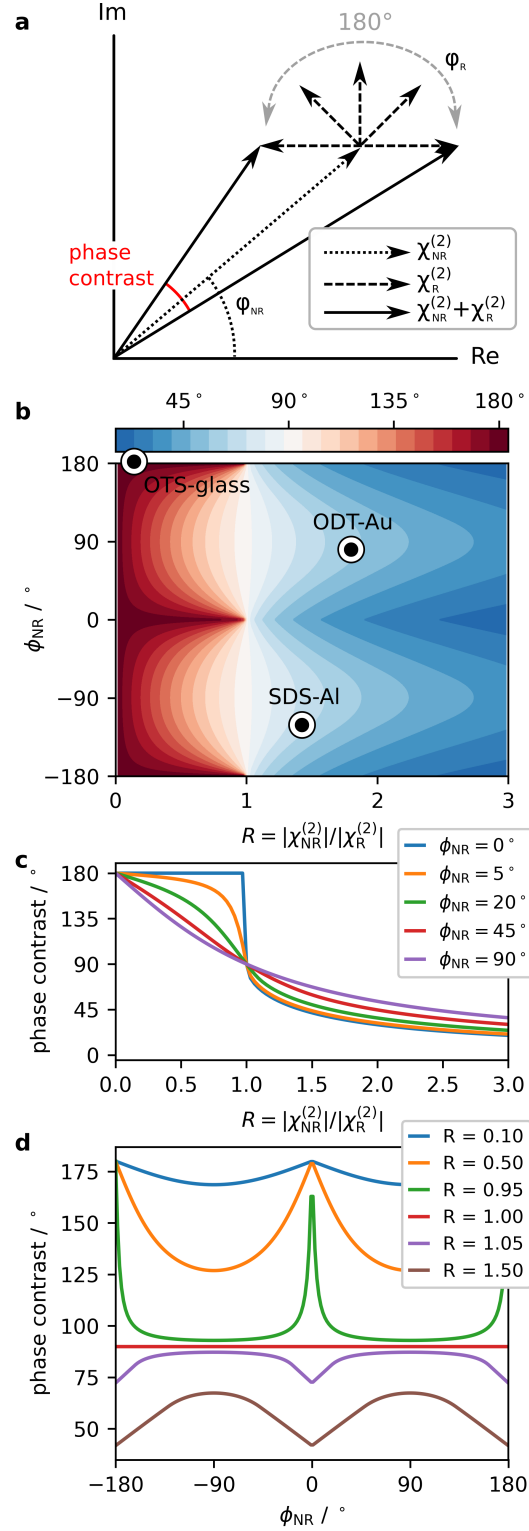
Figure 1: (a) Argand diagram illustrating the determination of the phase contrast, and (b) its predicted value according to the ratio of the non-resonant-to-resonant amplitude ratio and the non-resonant phase, ϕ_{NR}. (c) Some slices along the ϕ_{NR} direction and (d) $R = |\chi_{NR}^{(2)}|/|\chi_R^{(2)}|$ direction.

8

Bare metal surface

We first consider a heterodyne measurement of the aluminum surface exposed to air, where the local oscillator is generated in transmission from *y*-cut quartz. There are no vibrational resonances in the region 2800–3000 cm^{-1} (homodyne spectrum in Fig. 2a), but we do observe the interference between the LO and the SFG generated from the Al surface. Data obtained from an experiment where the IR beam frequency is scanned from 2800–3000 cm^{-1}, and the phase-shifting unit is rotated by 90° from −45 to +45° is used to obtain the phase information shown in Fig. 2b. The interference pattern appears much like one obtained for a transparent bulk nonlinear crystal such as *z*-cut quartz.[18] However, as the LO reflects off a metallic sample, and subsequently from a dielectric reference sample (*z*-cut quartz), an additional phase correction is required, as has been described in detail previously.[32] This has already been taken into account in presenting the phase data in Fig. 2b, using the frequency-dependent refractive index of aluminum. Using this analysis, we have determined that the phase of $\chi^{(2)}_{\text{NR}}$ for our aluminum sample is −120° throughout this region of the mid-infrared. This value depends on the visible wavelength and to the extent that the surface is clean. As the phase of this surface is not a multiple of 90°, the non-resonant component appears in both $\mathbb{R}\text{e}\{\chi^{(2)}\}$ and $\mathbb{I}\text{m}\{\chi^{(2)}\}$ as shown in the red and blue lines in Fig. 2c.

Glass-organic interface

For comparison, we present another simple case, trichloro(octadecyl)silane (OTS), functionalized onto a glass surface. Homodyne data appears in Fig. 2d. As there is negligible non-resonant SFG contribution, so the measured interference in a heterodyne experiment originates primarily between the vibrationally-resonant sample SFG and LO to yield the phase shown in Fig. 2e. The real and imaginary components of $\chi^{(2)}$ are indicated by the red and blue traces in Fig. 2f. If we fit this data assuming a model where each vibrational mode is represented by a Lorentzian line shape

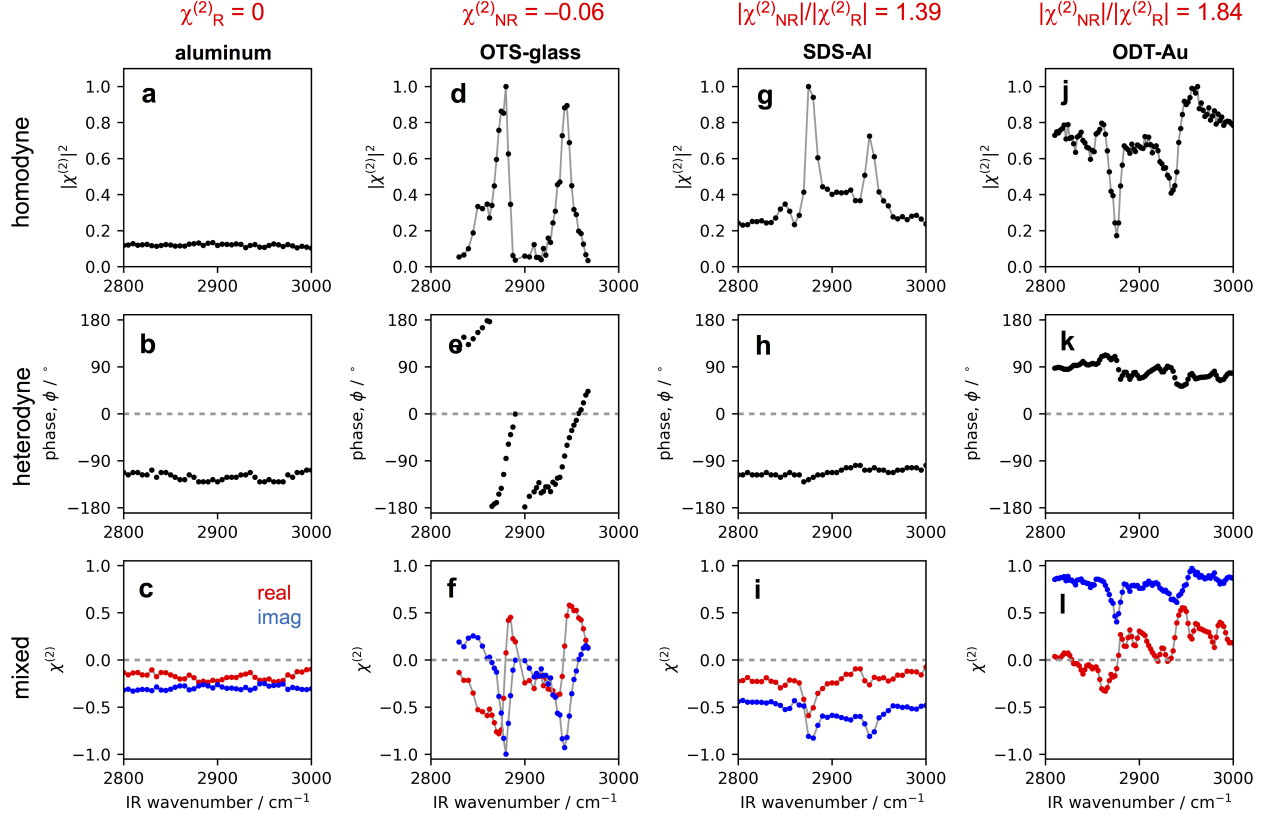$$\chi^{(2)}_{\text{R}}(\omega_{\text{IR}}) = \frac{A}{\omega_0 - \omega_{\text{IR}} - i\Gamma} \tag{4}$$

Figure 2: The top row shows homodyne SFG data obtained for the bare aluminum surface (left column), glass surface functionalized with OTS (second column), aluminum surface with adsorbed SDS (third column), and gold surface with covalently attached ODT (right column). The middle row shows the phase extracted from a heterodyne SFG experiment from the same four surfaces. The bottom row illustrates the real and imaginary components obtained from $|\chi^{(2)}|\cos\phi$ and $|\chi^{(2)}|\sin\phi$

where A is the (signed) amplitude of response, ω_0 is its resonant frequency, and Γ is the homogeneous linewidth, we can estimate the oscillator strength from the expression on resonance as A/Γ. For the methyl symmetric stretch, this produces a value of $R = -0.06$ as indicated by the annotation on Fig. 1b, with $\phi_{NR} = \pm 180°$. We therefore predict a phase contrast of nearly 180° on passing through this mode near 2875 cm^{-1}, in agreement with our observation.

Metal-organic interface

We now prepare a surface where sodium dodecyl sulfate (SDS) is adsorbed onto the same Al substrate we have previously characterized, and perform a homodyne SFG experiment. The measured signal is a superposition of the Al non-resonant and surfactant resonant contribution as

10

described in Eq. 1, and the measured intensity is given by

$$I \propto \left| |\chi_{NR}^{(2)}|e^{i\phi_{NR}} + |\chi_R^{(2)}|e^{i\phi_R} \right|^2$$

$$= |\chi_{NR}^{(2)}|^2 + |\chi_R^{(2)}|^2 + 2|\chi_{NR}^{(2)}||\chi_R^{(2)}|\cos(\phi_{NR} - \phi_R). \tag{5}$$

As the IR probe passes through a vibrational mode, we see a frequency dependence in the resonant contribution as in Eq. 4. The phase of the resonant component is given by

$$\phi_R(\omega_{IR}) = \arctan\left[\frac{A\Gamma}{A(\omega_0 - \omega_{IR})}\right].$$

Although it appears that the above expression may be independent of A, we have included it in the numerator and denominator, as the sign of A determines the quadrant of ϕ_R, a critical aspect of the phase characterization. In modelling such a response, it is therefore important to preserve the quadrant information in the inverse tangent operation. More explicitly,

$$\phi_R(\omega_{IR}) = \begin{cases} \arctan[\Gamma/(\omega_0 - \omega_{IR})] & \text{for } A > 0 \text{ and } \omega_{IR} < \omega_0 \\ \arctan[\Gamma/(\omega_0 - \omega_{IR})] + 180° & \text{for } A < 0 \text{ and } \omega_{IR} > \omega_0 \\ \arctan[\Gamma/(\omega_0 - \omega_{IR})] - 180° & \text{for } A < 0 \text{ and } \omega_{IR} < \omega_0. \end{cases} \tag{6}$$

An important conclusion here is that, when $\chi_{NR}^{(2)} = 0$, ϕ_R changes by 180° for an isolated vibrational mode upon passing through resonance. Examining the data Fig. 2g relatively far from any vibrational resonance (for example near 2800 cm^{-1}), $\chi_R^{(2)} \approx 0$ and $|\chi_{NR}^{(2)}| \approx \sqrt{I}$ from Eq. 5. Estimation of $|\chi_R^{(2)}|$ is not as straightforward as a result of the interference that is described by Eq. 5. However, from fitting the data to a sum of Lorentzians plus a non-resonant component, we have determined that $R = 1.39$. We then introduce the local oscillator to perform a heterodyne measurement. The extracted phase is shown in Fig. 2h, which bears a striking resemblance to that obtained for the bare Al surface (Fig. 2b), with a greatly diminished phase contrast largely blurring the strong vibrational features present in the homodyne data. If we were to combine this

phase information with $|\chi^{(2)}|$ obtained from the homodyne data in Fig. 2g, we can plot $\chi^{(2)} \cos \phi$ (red trace in Fig. 2i) and $\chi^{(2)} \sin \phi$ (blue trace) to obtain the real and imaginary components of $\chi^{(2)}$. In the case of dielectric substrates with negligible (or at least real-valued) $\chi_{NR}^{(2)}$, the sign of $\mathbb{Im}\{\chi^{(2)}\}$ reveals the polarity of the functional group, as will be described in more detail in the following section. Here a complex-valued non-resonant response contributes an offset to both the real and imaginary spectra, so it is now the direction of the band in $\mathbb{Im}\{\chi^{(2)}\}$, and not its sign, that is important.

Before generalizing our approach, we consider one final example of octadecylthiol (ODT) on gold, with the homodyne data in Fig. 2j. Gold has been widely used in SFG experiments as a phase reference, including applications where the metal is not in direct contact with the molecules of interest, but close enough to provide a source of non-resonant SFG. [23–25,36,37] For typical beam angles in a reflection experiment, the $|\chi_{NR}^{(2)}|$ for Au is at least two orders of magnitude weaker in ssp than in ppp polarization at 532 nm, often allowing $|\chi_{NR}^{(2)}|$ and $|\chi_R^{(2)}|$ to be comparable. [32] However, Fig. 2k again shows that the variation in phase is small. Fitting the data provides $R = 1.84$ for the methyl symmetric stretch, along with our direct measurement of $\phi = 84°$ from the heterodyne experiment. When this point is plotted on the map in Fig. 1b, one predicts a phase contrast of roughly $60°$, close to what is observed in our data. Note that our predictions in Fig. 1 are based on an isolated vibrational mode. When multiple modes spectrally interfere, the phase contrast is also diminished. Fig. 3 illustrates the measured magnitude and phase, and plots real and imaginary components of $\chi^{(2)}$ for the ODT-Au surface, as indicated by the points. Simultaneous fits to the magnitude and phase data resulted in the black lines. When the same set of Lorentzian amplitude, frequency, and width parameters are re-plotted without the non-resonant component, the predicted results are shown in red. From this comparison we can conclude that, although neighboring vibrational modes reduce the phase contrast, the effect is minor in comparison to the effect of the non-resonant contribution. We can see that the methyl symmetric stretch experiences a phase change of nearly $180°$ (red curve in Fig. 3b) if $\chi_{NR}^{(2)} = 0$, in comparison to the measured to phase contrast of ca. $60°$.
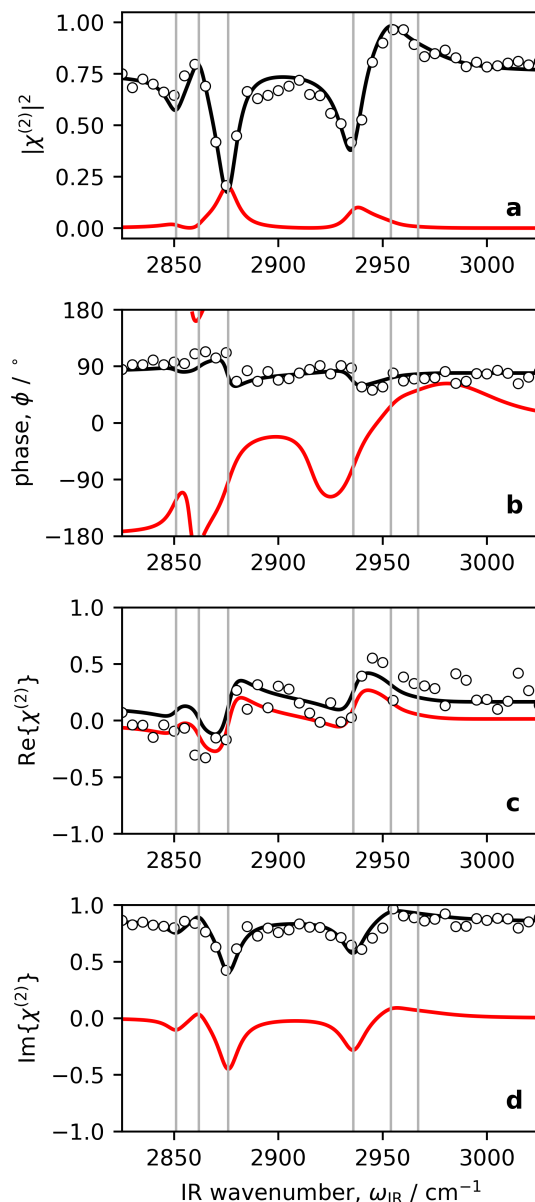
Figure 3: Experimental data in points obtained from a determination of the (a) magnitude squared and (b) phase of ODT on gold. These have been transformed into the (c) real and (d) imaginary components of $\chi^{(2)}$ (data in points). A fit to a model where each vibrational mode is represented by a Lorenztian is shown with black lines. The same model, but excluding the gold non-resonant contribution, is plotted with red lines.

Combined use of homodyne and heterodyne SFG data to establish functional group polarity

Although the above examples show that a complete treatment of the heterodyne data will yield the sought polarity information, it is useful to have a manner for extracting this from the homodyne data
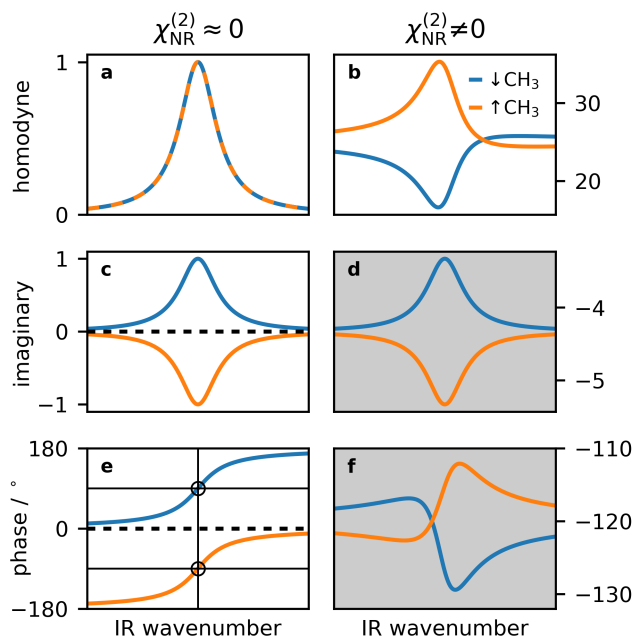
13

Figure 4: Illustration of the relationship between the apparent direction (upwards vs downwards pointing) of a vibrational resonance in homodyne and heterodyne SFG experiments. The first column $\chi_{NR}^{(2)} \approx 0$ represents situations with no non-resonant contribution; the second column shows the same resonance properties with a significant non-resonant background, with $\phi_{NR} = -120°$. Blue spectra are for the methyl symmetric stretch, where the C-to-H axis points towards the substrate. The same vibrational mode, but for the opposite polarity, is shown in orange. The shaded panels represent data that would be useful, but difficult to obtain in a heterodyne experiment.

directly in the case of strong non-resonant contributions that provide clear interference lineshapes. The relationship between all of the experiments and observables is summarized in Fig. 4. The left column represents the case of a molecule adsorbed on a surface with no significant non-resonant contribution; the right column presents the same case, but on a metallic substrate with $\phi_{NR} = -120°$ as in the case of aluminum. The first row depicts the result of a homodyne SFG experiment for a sample with methyl groups directed down (towards the substrate, indicate in blue) and up (away from the substrate, towards the vapor phase, indicated in orange). In the absence of any non-resonant contribution the two spectra are, of course, indistinguishable as seen in Fig. 4a. With a large non-resonant contribution (note the extent of the vertical axis in Fig. 4b), the two cases of methyl orientations are distinguishable. Practically, this occurs whenever $R > 1$. If a heterodyne experiment were performed on the dielectric substrate, the resonances would appear with opposite

14

signs (Fig. 4c) in the extracted imaginary component of the spectra, as we have shown in the case of OTS-glass. Alternatively, and a more direct representation of the measured quantity in the heterodyne experiment, the phase would change by 180°, passing through the resonance at either ±90°, depending on the methyl group orientation (Fig. 4e), as encoded in the sign of A. Although the corresponding data in the case of the metal substrate still reveal differences according to the polarity of the methyl group, the imaginary spectra are both negative in this case (Fig. 4d), and there is only a small change in phase (Fig. 4f) upon passing through the vibrational resonance. The phase contrast depends on the relative magnitudes $R = |\chi_{NR}^{(2)}|/|\chi_R^{(2)}|$ and ϕ_{NR}. Figs. 4d and 4f have been shaded to indicate that, although this information would lead to a determination of the methyl polarity, it is strictly not required, and may be difficult to obtain unless the experimental phase resolution is sufficiently high.

From an inspection of the SDS-Al and ODT-Au data, it is apparent that some phase information is present, but analysis hinges on the non-resonant phase. Furthermore, it has been demonstrated that the non-resonant phase of a metallic substrate may be substantially altered by the presence of the adsorbate, and is sensitive to the surface coverage.[38,39] However, if heterodyne measurements are available, ϕ_{NR} can be determined experimentally. In the presence of a strong non-resonant contribution, it is then practical and robust to obtain the chemical functional group polarity from the homodyne data. The relationship between the orientation and the direction/appearance of the corresponding resonance feature is given by the sign of $\cos(\phi_{NR} - \phi_R)$ as revealed by Eq. 5. If the nature of the SFG signal at that particular IR frequency is not certain, for example if multiple modes may contribute to the observed spectral feature, then both ϕ_{NR} and ϕ_R need to be determined in order to assess this. However, if it is known that the spectral feature is relatively free from contributions of other vibrational modes, a considerable simplification can be made, as was considered in the model in Fig. 4, where the phase changes by 180° upon passing through the resonance, and has a value of ±90° on resonance. In this case, we limit $\phi_R = \pm 90°$, and $\cos(\phi_{NR} - \phi_R)$ becomes $\pm \sin \phi_{NR}$.

We define a *polarity parameter P* as

$$P = \text{sgn}(A \cdot \sin \phi_{\text{NR}}) \tag{7}$$

where $P > 0$ indicates that a functional group pointing up will result in an "upward" resonance in a homodyne measurement. Taking the methyl symmetric stretch in ssp as an example, if the C-to-H axis is directed up, in the direction of the reflected SFG beam, the resonant amplitude in Eq. 6 is given by

$$
\begin{aligned}
A_{yyz} = {} & N(2\alpha_{ccc}^{(2)} + \alpha_{aac}^{(2)} + \alpha_{bbc}^{(2)})\langle\cos\theta\rangle \\
& - N(2\alpha_{ccc}^{(2)} - \alpha_{aac}^{(2)} - \alpha_{bbc}^{(2)})\langle\cos^3\theta\rangle
\end{aligned}
\tag{8}
$$

where a, b, c are the molecular frame Cartesian coordinates, with c along the methyl C_3 symmetry axis. In Fig. 5, harmonic approximations of these $\alpha^{(2)}$ elements are obtained for methyl groups in different environments. This method has been described in detail previously.[35] In brief, dipole moment vector and polarizability tensor elements (points indicated by open circles) are calculated for various geometries that represent vibration along the normal mode coordinate Q of interest, the methyl symmetric stretch in this case. Fits to second-order polynomials are indicated by solid lines; the slopes evaluated at $Q = 0$ are drawn with dashed lines. In all cases, $\partial\alpha_{aa}/\partial Q \approx \partial\alpha_{bb}/\partial Q$ and so, for the methyl symmetric stretch we can make the further approximation

$$
\begin{aligned}
A_{yyz} \approx {} & 2N\frac{\partial\mu_c}{\partial Q}\left[\frac{\partial\alpha_{aa}}{\partial Q} + \frac{\partial\alpha_{cc}}{\partial Q}\right]\langle\cos\theta\rangle \\
& + 2N\frac{\partial\mu_c}{\partial Q}\left[\frac{\partial\alpha_{aa}}{\partial Q} - \frac{\partial\alpha_{cc}}{\partial Q}\right]\langle\cos^3\theta\rangle \\
= {} & f_1\langle\cos\theta\rangle + f_3\langle\cos^3\theta\rangle
\end{aligned}
\tag{9}
$$

As Fig. 5 also reveals that $\partial\alpha_{aa,bb}/\partial Q > 0$, $\partial\alpha_{cc}/\partial Q < 0$, and $\partial\mu_c/\partial Q < 0$, and this results in $f_1 < 0$ and $f_3 < 0$. As a consequence, $A_{yyz} < 0$ when $0° < \theta < 90°$, and $A_{yyz} > 0$ when $90° < \theta < 180°$. On aluminum where $\phi_{\text{NR}} = -120°$, $\sin\phi_{\text{NR}} \approx -0.87$ and so P is positive.
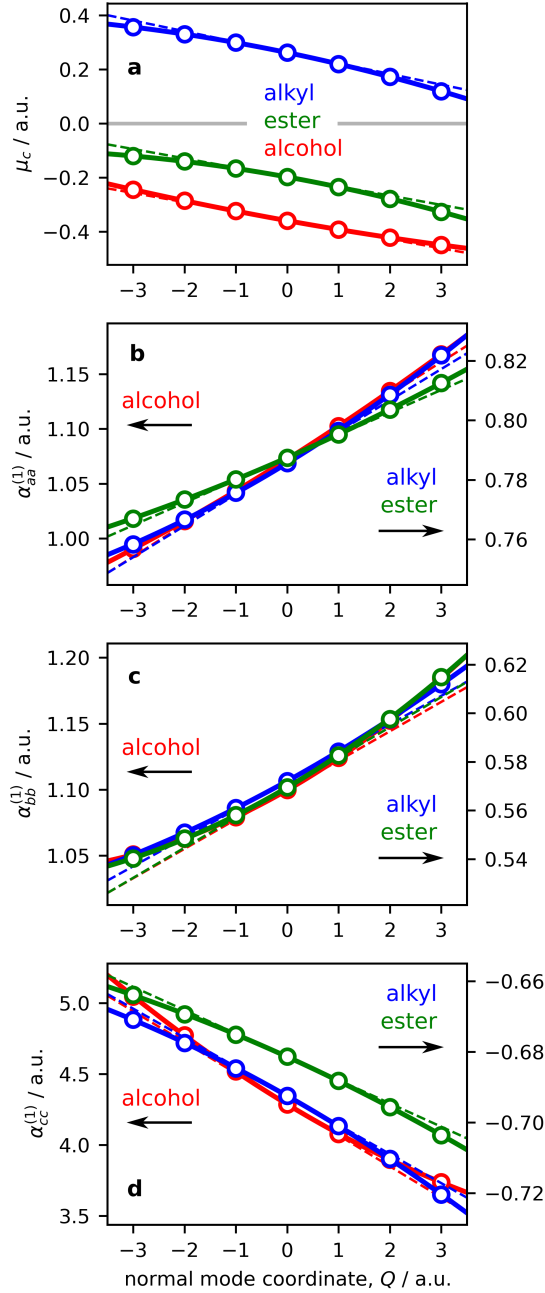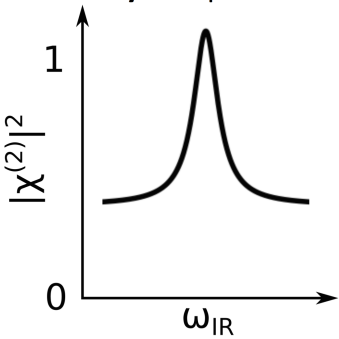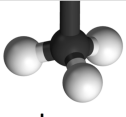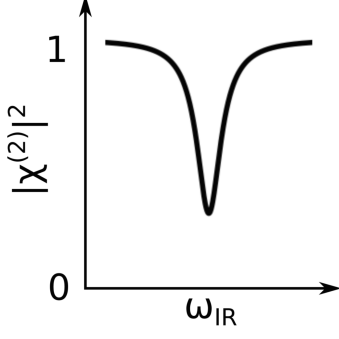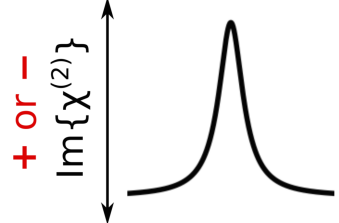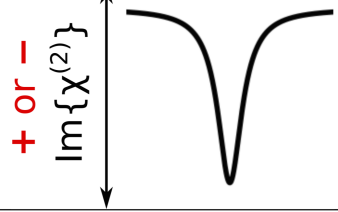
16

Figure 5: The relationship between the sign of the band in the $\mathrm{Im}\{\chi^{(2)}\}$ spectrum, or the direction of the band in the $|\chi^{(2)}|^2$ spectrum in the presence of significant non-resonant background, and the orientation of the chemical functional group depends on the sign of the relevant hyperpolarizability tensor elements. Here we illustrate that, for the methyl symmetric stretch, (a) $\partial\mu_c/\partial Q < 0$, (b,c) $\partial\alpha_{aa}/\partial Q \approx \partial\alpha_{bb}/\partial Q > 0$, and (d) $\partial\alpha_{cc}/\partial Q < 0$, regardless of whether the methyl group is part of an alkyl chain (blue), ester group (green), or alcohol (red). Points are the results of our calculation. Solid lines are the results of a fit to a second-order polynomial; dashed lines are the tangent evaluated at $Q = 0$.

17

In other words, an "upwards" band (as in the orange spectrum in Fig. 4b, and the experimental data in Fig. 2g) is predicted. In the case of the terminal methyl group of the ODT akyl chain on gold, $\phi_{NR} = 84°$ and $\sin \phi_{NR} \approx 1$. Examining the ODT-Au homodyne data in Fig. 2j, the CH_3 symmetric stretch is downwards pointing. Together with a negative value of P, we again come to the conclusion that the methyls are directed up, away from the gold surface. In the above discussion, we have simplified the consideration of which hyperpolarizability tensor elements in the molecular frame are projected onto the lab frame in the ssp experiment. We also point out that, while the signs of the $\alpha^{(2)}$ elements depend on the choice of molecular axes, the final conclusion does not. If the molecular frame were flipped so the hyperpolarizability elements are now providing a description of the molecule when it is upside down, the resulting tilt angle would now be the opposite quadrant, thereby describing the same molecular orientation. As a second example, if one considers the same hyperpolarizability calculation for the surface water free-OH stretch often observed near $3700 \ cm^{-1}$, one arrives at $A > 0$. Therefore the opposite conclusions are made from experimental data with similar appearance.

Table 1 summarizes the workflow for arriving at the polarity of a chemical functional group. In the case of a heterodyne experiment, the direction of $\mathbb{Im}\{\chi^{(2)}\}$ immediately provides the result, as long as the nature of the vibrational mode (from the magnitudes and signs of its relevent hyperpolarizability tensor elements) are known. This is a fundamental requirement for all SFG experiments that seek to establish the functional group polarity, contained in the A term. In the heterodyne experiment, the non-resonant phase only determines the sign of $\mathbb{Im}\{\chi^{(2)}\}$, and this information is irrelevant for our purpose. It is more interesting to consider the homodyne experiment, as the signal-to-noise is high, the measurement is easy and quick to perform, and the analysis is less susceptible to error. Note that the homodyne data we are describing here applies only in the case of a significant non-resonant background with known phase. Here the product of the signs of A and ϕ_{NR} determine the sign of the polarity parameter. A positive value of P indicates that the direction of the peak in the homodyne data indictes the direction of the functional group orientation. If P is negative, the connection is reversed.

Table 1: Scheme for determining the polarity of a chemical function group based on either a homodyne measurement (when there is significant non-resonant amplitude), or a heterodyne measurement. In all cases, a coincident external reflection geometry is assumed, where methyls pointing up have their C-to-H vector parallel to the reflected SFG beam.

Experiment / observation	mode character	NR phase $-180° < \phi < 180°$	polarity parameter	orientation
homodyne "upwards" — $|\chi^{(2)}|^2$ vs ω_{IR} (upward peak)	A < 0 methyl	$\phi > 0°$ gold	−	down
	A < 0 methyl	$\phi < 0°$ aluminum	+	up
	A > 0 free OH	$\phi > 0°$ gold	+	up
	A > 0 free OH	$\phi < 0°$ aluminum	−	down
homodyne "downwards" — $|\chi^{(2)}|^2$ vs ω_{IR} (downward dip)	A < 0 methyl	$\phi > 0°$ gold	−	up
	A < 0 methyl	$\phi < 0°$ aluminum	+	down
	A > 0 free OH	$\phi > 0°$ gold	+	down
	A > 0 free OH	$\phi < 0°$ aluminum	−	up
heterodyne "upwards" — + or − $\mathrm{Im}\{\chi^{(2)}\}$ (upward peak)	A < 0 methyl	not important		down
	A > 0 free OH			up
heterodyne "downwards" — + or − $\mathrm{Im}\{\chi^{(2)}\}$ (downward dip)	A < 0 methyl	not important		down
	A > 0 free OH			up

Conclusions

Phase-resolved SFG spectroscopy is a powerful tool for elucidating the structure of molecules on surfaces that is uniquely capable of resolving the polarity of each chemical group orientation, i.e. distinguishing the quadrants that define the up vs down directions. This technique has been especially valued for the study of dielectric surfaces, where the lack of a non-resonant contribution offers few other clues to the polarity, as interference effects are generally weak or non-existent. On metal surfaces, phase-resolved experiments also provide information of the surface electronic structure, which is in turn sensitive to the nature and coverage of adsorbed species. However, there are practical challenges associated with measuring the resonant phase on metal surfaces, as the phase contrast is observed (and anticipated) to be low. One solution to this problem is to use the phase of the metal (preferably in the presence of the absorbed molecules) as determined in a heterodyne scheme, together with the homodyne data, in order to extract the sought polarity, as an alternative to retrieving the complete imaginary spectrum.

Acknowledgement

References

(1) Liu, W.; Tkatchenko, A.; Scheffler, M. Modeling Adsorption and Reactions of Organic Molecules at Metal Surfaces. *Acc. Chem. Res.* **2014**, *47*, 3369–3377.

(2) Casford, M. T.; Davies, P. B. The Structure of Oleamide Films at the Aluminum/Oil Interface and Aluminum/Air Interface Studied by Sum Frequency Generation (SFG) Vibrational Spectroscopy and Reflection Absorption Infrared Spectroscopy (RAIRS). *ACS Appl. Mater. Chem.* **2009**, *8*, 1672–1681.

(3) Duffy, D. C.; Friedmann, A.; Boggis, S. A.; Klenerman, D. Surface vibrational spectroscopy of lubricants adsorbed at the iron-water interface. *Langmuir* **1998**, *14*, 6518–6527.

(4) Chen, X.; Clarke, M. L.; Wang, J.; Chen, Z. Sum Frequency Generation Vibrational Spectroscopy Studies on Molecular Conformation and Orientation of Biological Molecules at Interfaces. *International Journal of Modern Physics B* **2005**, *19*, 691–713.

(5) Malik, M. A.; Ali, M.; Nabi, F.; Al-Thabaiti, S. A.; Khan, Z. Anti-corrosion Ability of Surfactants: A Review. *Int. J. Electrochem. Sci.* **2011**, *6*, 1927–1948.

(6) Pogrzeba, T.; Schmidt, M.; Milojevic, N.; Urban, C.; Illner, M.; Repke, J.-U.; Schomäcker, R. Understanding the Role of Nonionic Surfactants during Catalysis in Microemulsion Systems on the Example of Rhodium-Catalyzed Hydroformylation. *Ind. Eng. Chem. Res.* **2017**, *56*, 9934–9941.

(7) Stolle, R.; Marowsky, G.; Schwarzberg, E.; Berkovic, G. Phase Measurement in Nonlinear Optics. *Appl. Phys. B* **1996**, *63*, 491–498.

(8) Superfine, R.; Huang, J. Y.; Shen, Y. R. Phase Measurement For Surface Infrared-Visible Sum-Frequency Generation. *Opt. Lett.* **1990**, *15*, 1276–1278.

(9) Shen, Y. R.; Ostroverkhov, V. Sum-frequency Vibrational Spectroscopy on Water Interfaces: Polar Orientation of Water Molecules at Interfaces. *Chem. Rev.* **2006**, *106*, 1140–1154.

(10) Han, Y.; Raghunathan, V.; ran Feng, R.; Maekawa, H.; Chung, C.-Y.; Feng, Y.; Potma, E. O.; Ge, N.-H. Mapping Molecular Orientation with Phase Sensitive Vibrationally Resonant Sum-Frequency Generation Microscopy. *J. Phys. Chem. B* **2013**, *117*, 6149–6156.

(11) Schwarzberg, E.; Berkovic, G.; Marowsky, G. Nonlinear interferometry and phase measurements for surface second-harmonic generation in a dispersive geometry. *Appl. Phys. A* **1994**, *59*, 631–637.

(12) Chang, R. K.; Ducuing, J.; Bloembergen, N. Relative phase measurement between fundamental and second-harmonic light. *Phys. Rev. Lett.* **1965**, *15*, 6–8.

(13) Carriles, R.; An, Y. Q.; Downer, M. C. Frequency-domain measurement of second harmonic phase. *Phys. Stat. Sol.* **2005**, *242*, 3001–3006.

(14) Chen, J.; Machida, S.; Yamanoto, Y. Simultaneous measurement of amplitude and phase in surface second-harmonic generation. *Opt. Lett.* **1998**, *23*, 676–678.

(15) Kajikawa, K.; Wang, L.-M.; Isoshima, T.; Wada, T.; Knoll, W.; Sasabe, H.; Okada, S.; Nakanishi, H. Phase measurement of second-harmonic generation reveals the directional sense of a 2-docosylamino-5-nitropyridine (DCANP) molecule in Langmuir–Blodgett films. *Thin Solid Films* **1996**, *284–285*, 612–614.

(16) Lu, R.; Rao, Y.; Zhang, W.-K.; Wang, H.-F. Phase Measurement in Nonlinear Optics of Molecules at Air/Water Interface with Femtosecond Laser Pulses. *Proc. SPIE Conf. Nonlinear. Spectrosc.* **2002**, *4812–4815*, 115–124.

(17) Mifflin, A.; Musorrafiti, M.; Konek, C.; Geiger, F. Second harmonic generation phase measurements of Cr(VI) at a buried interface. *J. Phys. Chem. B* **2005**, *109*, 24386–24390.

(18) Jena, K. C.; Covert, P. A.; Hore, D. K. Phase Measurement in Non-Degenerate Three-Wave Mixing Spectroscopy. *J. Chem. Phys.* **2011**, *134*, 044712.

(19) Covert, P. A.; FitzGerald, W. A.; Hore, D. K. Simultaneous Measurement of Magnitude and Phase in Interferometric Sum-Frequency Vibrational Spectroscopy. *J. Chem. Phys.* **2012**, *137*, 014201.

(20) Ji, N.; Ostroverkhov, V.; Chen, C.; Shen, Y. R. Phase-Sensitive Sum-Frequency Vibrational Spectroscopy and its Application to Studies of Interfacial Alkyl Chains. *J. Am. Chem. Soc.* **2007**, *129*, 10056–10057.

(21) Wang, J.; Bisson, P. J.; Marmolejos, J. M.; Shultz, M. J. Measuring Complex Sum Frequency Spectra with a Nonlinear Interferometer. *J. Phys. Chem. Lett.* **2016**, *7*, 1945–1949.

(22) Yamaguchi, S. Development of Single-Channel Heterodyne-Detected Sum Frequency Generation Spectroscopy and its Application to the Water/Vapor Interface. *J. Chem. Phys.* **2015**, *143*, 034202.

(23) Rich, C. C.; Lindberg, K. A.; Krummel, A. T. Phase Acrobatics: The Influence of Excitonic Resonance and Gold Nonresonant Background on Heterodyne-Detected Vibrational Sum Frequency Generation Emission. *J. Phys. Chem. Lett.* **2017**, *8*, 1331–1337.

(24) Ward, R. N.; Davies, P. B.; Bain, C. D. Orientation of Surfactants Adsorbed on a Hydrophobic Surface. *J. Phys. Chem.* **1993**, *97*, 7141–7143.

(25) Weidner, T.; Apte, J. S.; Gamble, L. J.; Castner, D. G. Probing the Orientation and Conformation of α-Helix and β-Strand Model Peptides on Self-Assembled Monolayers Using Sum Frequency Generation and NEXAFS Spectroscopy. *Langmuir* **2009**, *26*, 3433–3440.

(26) Cimatu, K.; Baldelli, S. Chemical Imaging of Corrosion: Sum Frequency Generation Imaging Microscopy of Cyanide on Gold at the Solid-Liquid Interface. *J. Am. Chem. Soc.* **2008**, *130*, 8030–8037.

(27) Zhang, H.; Romero, C.; Baldelli, S. Preparation of Alkanethiol Monolayers on Mild Steel Surfaces Studied with Sum Frequency Generation and Electrochemistry. *J. Phys. Chem. B* **2005**, *109*, 15520–15530.

(28) Miyamae, T. In *Vibrational Spectorscopy*; de Caro, D., Ed.; InTech: Rijeka, 2012; Vol. 5; pp 115–140.

(29) Jang, J. H.; Lydiatt, F.; Lindsay, R.; Baldelli, S. Quantitative Orientation Analysis by Sum Frequency Generation in the Presence of Near-Resonant Background Signal: Acetonitrile on Rutile TiO$_2$ (110). *J. Phys. Chem. A* **2013**, *117*, 6288–6302.

(30) Fang, M.; Baldelli, S. Surface-Induced Heterogeneity Analysis of an Alkanethiol Monolayer on Microcrystalline Copper Surface Using Sum Frequency Generation Imaging Microscopy. *J. Phys. Chem. C* **2017**, *121*, 1591–1601.

(31) Liu, Y.; Wolf, L. K.; Messmer, M. C. A study of alkyl chain conformational changes in self-assembled *n*-octadecyltrichlorosilane monolayers on fused silica surfaces. *Langmuir* **2001**, *17*, 4329–4335.

(32) Covert, P. A.; Hore, D. K. Assessing the Gold Standard: The Complex Vibrational Nonlinear Susceptibility of Metals. *J. Phys. Chem. C* **2015**, *119*, 271–276.

(33) Bain, C. D.; Troughton, E. B.; Tao, Y.-T.; Evall, J.; Whitesides, G. M.; Nuzzo, R. G. . Formation of Monolayer Films by the Spontaneous Assembly of Organic Thiols from Solution onto Gold. *J. Am. Chem. Soc.* **1989**, *111*, 321–335.

(34) Jena, K. C.; Covert, P. A.; Hall, S. A.; Hore, D. K. Absolute Orientation of Ester Side Chains on the PMMA Surface. *J. Phys. Chem. C* **2011**, *115*, 15570–15574.

(35) Hall, S. A.; Hickey, A. D.; Hore, D. K. Structure of Phenylalanine Adsorbed on Polystyrene From Nonlinear Vibrational Spectroscopy Measurements and Electronic Structure Calculations. *J. Phys. Chem. C* **2010**, *114*, 9748–9757.

(36) Breen, N. F.; Weidner, T.; Li, K.; Castner, D. G.; Drobny, G. P. A solid-state deuterium NMR and sum-frequency generation study of the side-chain dynamics of peptides adsorbed onto surfaces. *J. Am. Chem. Soc.* **2009**, *131*, 14148–14149.

(37) Weidner, T.; Breen, N. F.; Li, K.; Drobny, G. P.; Castner, D. G. Sum Frequency Generation and

Solid-State NMR Study of the Structure, Orientation, and Dynamics of Polystyrene-Adsorbed Peptide. *Proc. Natl. Acad. Sci. U.S.A.* **2010**, *107*, 13288–13293.

(38) Buck, M.; Eisert, F.; Grunze, M.; Trager, F. Second-Order Nonlinear Susceptibilites of Surfaces. *Appl. Phys. A.* **1995**, *60*, 1–12.

(39) Dreesen, L.; Humbert, C.; Celebi, M.; Lemaire, J. J.; Mani, A. A.; Thiry, P. A.; Peremans, A. Influence of the Metal Electronic Properties on the Sum-Frequency Generation Spectra of Dodecanethiol Self-Assembled Monolayers on Pt (111), Ag (111) and Au (111) Single Crystals. *Appl. Phys. B* **2002**, *74*, 621–625.

Graphical TOC Entry
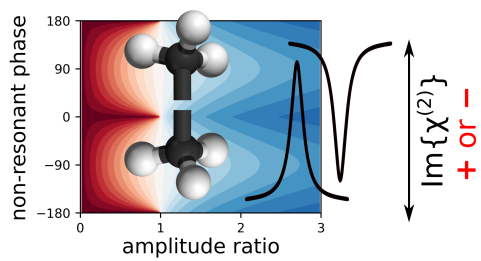
Correction to "Determining the Orientation of Chemical Functional Groups on Metal Surfaces by a Combination of Homodyne and Heterodyne Nonlinear Vibrational Spectroscopy"

Wei-Chen Yang and Dennis K Hore*

Department of Chemistry, University of Victoria, Victoria, British Columbia V8W 3V6, Canada
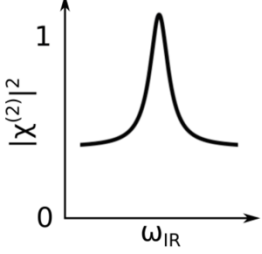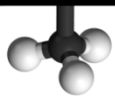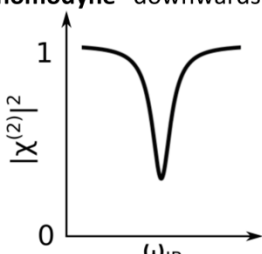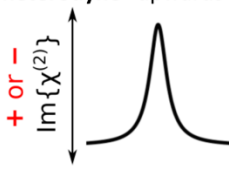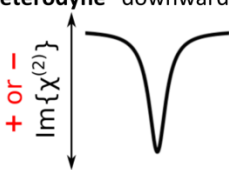
We would like to make one correction and one clarification to Table 1 summarizing the results of our recent article.[1] We made an error in the last column of the last two rows describing the "heterodyne, downwards" case. The entry "A < 0" should have been listed as "orientation up"; the "A > 0" entry should have been described as "orientation down". We sincerely regret this error, as the point of the table was to summarize our findings in a clear way, and alleviate some confusion in the field.

We would also like to take this opportunity to clarify the presentation. The original version of the table described the "mode character" in terms of the quantity A. Some feedback that we have received since this was published has convinced us that it would be better to label the mode character with a + or −, more consistent with the definition of A in the text.

References

1. Yang, W.-C.; Hore, D. K. Determining the Orientation of Chemical Functional Groups on Metal Surfaces by a Combination of Homodyne and Heterodyne Nonlinear Vibrational Spectroscopy. *J. Phys. Chem. C* **2017**, 121, 208043–28050.

Table 1. Scheme for Determining the Polarity of a Chemical Function Group Based on Either a Homodyne Measurement (when there is significant nonresonant amplitude) or a Heterodyne Measurement[a]

Experiment / observation	mode character	NR phase $-180° < \phi < 180°$	polarity parameter	orientation
homodyne "upwards" (plot of $|\chi^{(2)}|^2$ vs ω_{IR}, peak)	− methyl C → H	$\phi > 0°$ gold	−	$\theta > 90°$ C → H down
		$\phi < 0°$ aluminum	+	$\theta < 90°$ C → H up
	+ free OH O → H	$\phi > 0°$ gold	+	$\theta < 90°$ O → H up
		$\phi < 0°$ aluminum	−	$\theta > 90°$ O → H down
homodyne "downwards" (plot of $|\chi^{(2)}|^2$ vs ω_{IR}, dip)	−	$\phi > 0°$ gold	−	$\theta < 90°$
		$\phi < 0°$ aluminum	+	$\theta > 90°$
	+	$\phi > 0°$ gold	+	$\theta > 90°$
		$\phi < 0°$ aluminum	−	$\theta < 90°$
heterodyne "upwards" (plot of $+$ or $-$ $\mathrm{Im}\{\chi^{(2)}\}$, peak)	−	not required		$\theta > 90°$
	+			$\theta < 90°$
heterodyne "downwards" (plot of $+$ or $-$ $\mathrm{Im}\{\chi^{(2)}\}$, dip)	−			$\theta < 90°$
	+			$\theta > 90°$

[a]The *mode character* refers to sign of the hyperpolarizability tensor elements, prior to their rotation in the lab frame. In all cases, a coincident external reflection geometry is assumed, where methyls pointing up have their C-to-H vector parallel to the reflected SFG beam.